Analyzing the liquid state of two-dimensional dust clusters: The instantaneous normal mode approach

André Melzer and André Schella
Institut für Physik, Ernst-Moritz-Arndt-Universität Greifswald, 17489 Greifswald, Germany

Jan Schablinski, Dietmar Block, and Alexander Piel
Institut für Experimentelle und Angewandte Physik, Christian-Albrechts-Universität zu Kiel, 24098 Kiel, Germany
(Received 10 January 2013; published 25 March 2013)

The liquid state and the freezing transition of finite two-dimensional dust systems are studied using the instantaneous normal mode (INM) analysis. This technique measures the instantaneous unstable modes of a cluster configuration and relates them to the liquid properties of the system. Here, the INM analysis has been applied to experiments on laser-heated dust clusters. From the experiments, diffusion constants and melting temperatures for clusters of different size have been derived. The INM diffusion constants have been compared to those derived from other standard approaches. The scatter of the diffusion constant retrieved by the INM is smaller than that retrieved by other methods, allowing a more reliable determination of melting temperatures. Moreover, the behavior of double-well and escape modes, which reflect certain topological properties of unstable modes, correlates very well with the behavior of the diffusion constant. Further, the dynamic nature of the unstable modes has been determined as mostly shearlike. Finally, the INM results on the experiments are checked against those from Langevin simulations.

DOI: 10.1103/PhysRevE.87.033107 PACS number(s): 52.27.Lw, 64.60.an

I. INTRODUCTION

Dusty plasmas provide an ideal situation in which to study the dynamical processes of charged-particle systems. Dust particles can be followed on the kinetic level of individual particles because the temporal and spatial scales in dust systems can easily be resolved by video microscopy. Further, the dynamical properties are only weakly damped by the gaseous plasma environment. In a plasma, the particles attain high negative charges of the order of a few thousand elementary charges, resulting in a dominance of the mutual electrostatic interaction over the thermal motion. Hence, these systems are usually strongly coupled and arrange in an ordered, crystalline state [1–3].

For melting, the particles in these dusty plasmas have to be effectively heated. Focused laser beams can be used to manipulate the dust particles by radiation pressure effects; see, e.g., [4–8]. Random laser excitation can effectively mimic a heating process from an ordered solidlike state to a fluid state [9,10]. In recent experiments and simulations, a laser technique was described that provides true equilibrium heating of a two-dimensional (2D) dust system [11,12]. This now allows us to address the influence of unstable mode dynamics during solid-fluid phase transitions which otherwise might be masked by the nonequilibrium nature of the heating process.

Finite systems (clusters) add an interesting feature to the problem of phase transitions, namely the boundary effects due to the confinement potential. Finite systems of confined dust particles in dusty plasmas can be prepared in two dimensions [13–17] or three dimensions [18–20]. In finite systems, the melting is a two-step process, in which first orientational order is lost and, in a second step at a higher temperature, radial order is destroyed [21–23]. Furthermore, due to the finite system size, the thermodynamic quantities do not show a sharp transition [24,25]. Combining the aspects of full dynamic information, weak damping, equilibrium laser heating, and finite system size, finite two-dimensional dust clusters represent interesting systems in which to study the effects of phase transitions.

In a recent paper [26], we applied the instantaneous normal mode (INM) technique [27–31] to derive the freezing temperatures of experimental finite 2D dust clusters. The INM analysis was originally developed to determine diffusion constants or solvation properties in (simulated) extended liquids, especially for the case of supercooled liquids or liquids near freezing [27–31]. With our laser-heated dust clusters, we were then able to demonstrate the usefulness of the INM technique for our experimental finite dust systems. Here, we will show that the INM analysis provides an interesting approach to evaluate the fluid side of the phase transition for finite dust clusters in the experiments. The dynamic nature of the unstable instantaneous modes will be discussed, and comparisons to standard measures of diffusion constants will be performed. The unstable modes will be filtered according to topological criteria, and their correlation with the diffusion constants will be studied. The experiments will be complemented by Langevin simulations of dust clusters.

II. INSTANTANEOUS NORMAL MODE ANALYSIS

Dynamical processes of a finite ensemble of particles can be addressed by an analysis of the normal modes [16,32–35]. The normal modes are derived from a harmonic approximation to the potential energy surface around the equilibrium configuration. They are computed as the eigenvalues and eigenvectors of the dynamical matrix (Hessian) of the energy, i.e.,

$$\mathbf{A} = \left(\frac{\partial^2 E}{\partial r_{i\alpha} \partial r_{j\beta}} \right), \tag{1}$$

with $\alpha,\beta = \{x,y\}$ denoting $r_{i\alpha}$ as the x or y coordinate of particle i. The eigenvalues ω_ℓ^2 of $\mathbf{A}$ are the square of the eigenfrequencies ω_ℓ and the eigenvector $\vec{e}_\ell$ describes the oscillation pattern of the particles in mode number ℓ. The energy of dust clusters is usually described as a finite charged-particle system trapped in a harmonic confinement, i.e.,

$$E = \frac{1}{2}m\omega_0^2\sum_i^N r_i^2 + \frac{Z^2e^2}{4\pi\epsilon_0}\sum_{i<j}^N \frac{\exp(-r_{ij}/\lambda_\mathrm{D})}{r_{ij}}, \qquad (2)$$

where r_{ij} is the distance between particles i and j. The dust mass is denoted by m and the dust charge number by Z. Further, e is the elementary charge and ϵ_0 is the vacuum permittivity. The first term describes the potential energy in the confining potential of strength ω_0 and the second term is the Coulomb repulsion between the particles, including shielding by the ambient plasma with the Debye shielding length λ_D. Other influences, such as ion-streaming-induced dynamics, do not need to be considered for these single-layer systems [12,16].

In normalized energy units $E_0 = [Z^4e^4m\omega_0^2/(32\pi\epsilon_0)]^{1/3}$ and scale lengths $r_0 = [Z^2e^2/(2\pi\epsilon_0 m\omega_0^2)]^{1/3}$, the energy is simply written as

$$E = \sum_i^N r_i^2 + \sum_{i<j}^N \frac{\exp(-\kappa r_{ij})}{r_{ij}} \qquad (3)$$

with the screening strength $\kappa = r_0/\lambda_\mathrm{D}$ [21,32,36,37].

The instantaneous normal mode (INM) analysis [27–31,38] tries to connect the curvature of the energy landscape of momentary configurations to the dynamic properties of a liquid state such as the diffusion constant. For the calculation of the INM, the dynamical matrix $\mathbf{A}$ is calculated for every instantaneous configuration. In the liquid state, instantaneous configurations close to equilibrium result in the expected positive values for the eigenvalues ω_ℓ^2 similar to those of the solid state. However, when the liquid instantaneous configuration deviates from equilibrium, negative eigenvalues ω_ℓ^2 of the dynamical matrix may be found. Hence, the normal mode frequencies ω_ℓ are either purely real (reflecting the stable, equilibrium modes) or purely imaginary (reflecting the nonequilibrium, unstable modes), respectively.

The resulting density of states,

$$\rho(\omega) = \left\langle \sum \delta(\omega - \omega_\ell) \right\rangle, \qquad (4)$$

is the averaged distribution of the normal mode frequencies with the normalization $\int d\omega\, \rho(\omega) = 1$. The total density of states can be split into the stable part $\rho_s(\omega)$ with real ω_ℓ and the unstable part $\rho_u(\omega)$ with imaginary ω_ℓ.

Real values of ω_ℓ correspond to potential wells in the momentary energy landscape of the system, in which the particles can oscillate around their current equilibrium in the cage of the nearest neighbors. Imaginary values of ω_ℓ correspond to the potential hills that separate the minima. It is now argued [27–30,38] that especially the unstable part can be related to the liquid properties, such as the diffusion constant D, since the thermal energy drives configurational transitions to take place over these potential hills associated with $\rho_u(\omega)$. According to this reasoning, the diffusion constant is given as [27–30,38]

$$D = \frac{k_\mathrm{B}T}{m}\int \rho(\omega)\frac{\tau_h}{1+\tau_h^2\omega^2}d\omega, \qquad (5)$$

where τ_h is the average waiting time that is associated with the transition across potential barriers to other local minima in the momentary many-body potential surface of the liquid (see also Ref. [39]). The waiting time is given by

$$\tau_h^{-1} = \int \frac{\omega}{2\pi}\frac{Q_B}{Q_m} s n(\omega)\exp[-\beta E_B(\omega)]d\omega, \qquad (6)$$

where $\beta = 1/(kT)$ with the temperature T and Boltzmann's constant k, $E_B(\omega)$ is the characteristic barrier height for barrier frequency ω, s is the number of saddles in the potential surface connected to each potential well, $n(\omega)$ is the normalized distribution of saddle frequencies, and, finally, Q_B, Q_m are the partition functions of stable modes in the barrier and the well, respectively.

Following the method of Vijayadamodar and Nitzan [30], the hopping frequency τ_h^{-1} can be simplified as

$$\tau_h^{-1} = c\int \frac{\omega}{2\pi}\rho(\omega)\, A\exp\left(-B\frac{\omega^2}{kT}\right)d\omega, \qquad (7)$$

where $c \approx 3$ is associated with the different possibilities of escape routes from a potential minimum. In their model, the dependencies of $E_B(\omega)$, $n(\omega)$, and Q_B/Q_m can be summarized into the exponential form $A\exp(-B\omega^2/kT)$, where the parameters A and B are obtained from fitting $\rho_u(|\omega|)/\rho_s(\omega)$ to this exponential function. This is the basic INM technique taking into account all unstable modes.

The modes in the unstable part $\rho_u(\omega)$ can be further refined with respect to their topological properties (see, for example, Ref. [40]). It has been shown that some of the imaginary frequency modes are not connected to diffusion [31]. This is because imaginary frequencies ω_ℓ can result either from double-well potentials where the imaginary frequencies correspond to the barrier between two stable wells or from shoulder modes that result from a single well with a shoulder of negative curvature. These latter modes do not describe transition over an energy barrier, whereas the double wells (DWs) are those which might be considered to contribute primarily to diffusion. To extract only those INMs that are connected to double wells, the energy E of Eq. (2) is calculated along the eigenvectors $\vec{e}_\ell$ of each mode ℓ with imaginary ω_ℓ. By tracing the energy along the eigenvectors, double wells can be separated from shoulder modes.

A further, more advanced filtering addresses the question of whether the two minima of a DW mode really belong to different configurations. For that purpose, the pair of one-dimensional minima of the double well along $\vec{e}_\ell$ are traced to the minima in the $2N$-dimensional energy landscape. Then the $2N$-dimensional distance between the minima is determined. Modes that then correspond to two different $2N$ minima are termed escape or true DW modes (see, e.g., [40]).

In the analysis below, we will discuss the influence of this topological mode filtering, i.e., the use of *all* or of the refined *double well* or of the *escape* modes.

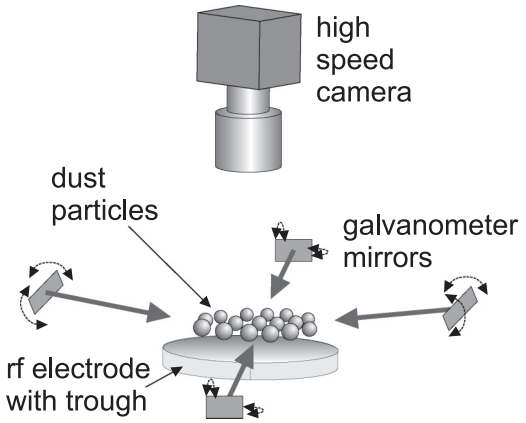

FIG. 1. Scheme of the experimental setup. Four heating laser beams are swept by galvanometer mirrors randomly over the dust cluster. The particle motion is recorded by a high-speed camera. See also [11].

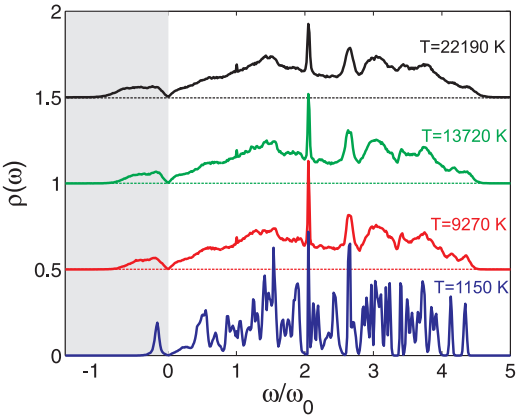

FIG. 2. (Color online) Density of states for a cluster with $N = 26$ at four different temperatures. The gray area indicates the unstable branch ρ_u containing the imaginary values of ω_ℓ, where $\rho_u(\omega)$ is plotted as $\rho_u(|\omega|)$ on the negative frequency axis ($\omega \to -|\omega|$).

III. EXPERIMENT

The experiment to laser-heat the finite dust clusters is described in detail in Ref. [11]. Here, only the main points are repeated for clarity. The experiments have been performed in a parallel plate radio-frequency (rf) discharge at 13.56 MHz. The discharge was operated in argon at a gas pressure of 7 Pa and at an rf power of 3 W. Dust particles (plastic melamine-formaldehyde microspheres) of 12.26 μm diameter were trapped in the space-charge sheath above the lower electrode. The electrode was equipped with a shallow spherical depression to confine the particles horizontally; see also Fig. 1. The particle motion was recorded via a top-view camera at a frame rate of 60 frames per second (fps). In a typical run, the particle motion was recorded for 250 s corresponding to 15 000 frames.

To heat the dust particles, a four-axis laser heating system was used [11] in which two pairs of opposing beams run from each of the two horizontal directions. The beams were swept independently and randomly over the cluster area. A thermal Brownian motion is realized in such a way that the time for every sweep over the cluster is chosen randomly. This random sweep time heating together with the excitation from all four horizontal directions guarantees a true thermodynamic heating of the cluster [11,12]. This means that the particle velocities are truly Maxwellian and isotropic. The power spectra of particle motion do not show any sign of preferred excitation of certain frequencies.

Hence, this true equilibrium heating method is a prerequisite for the identification of unstable modes from the particle trajectories which otherwise might be due to the nonequilibrium nature of heating.

IV. RESULTS

Here, we present an INM analysis of 2D dust clusters heated by our four-axis laser system. The INM analysis will be illustrated in the following mainly for a cluster of $N = 26$ particles. The results are qualitatively identical for the other clusters with $N = 19$ to 50 in the experiment; compare Ref. [26].

A. INM analysis

We start with an illustration of the INM method to determine the liquid properties of the observed finite dust clusters. For the analysis, video sequences of 15 000 frames at 60 fps were recorded for each temperature value realized by the four-axis laser heating system. For the $N = 26$ cluster, 12 different temperatures of the cluster between room temperature and $T = 22\,190$ K have been acquired. Since the laser-heating provides Maxwellian velocity distributions [11], the kinetic temperature (in two dimensions) is simply $kT = m\langle v_x^2 + v_y^2\rangle/2$.

Now, for each temperature setting, the dynamical matrix $\mathbf{A}$ as well as its eigenvalues and eigenvectors are calculated for each of the 15 000 time steps using the instantaneous particle positions $\vec{r}_i(t)$ for the calculation of the energy E according to Eq. (3). The number of instantaneous eigenvalues (and eigenvectors) then is $2N \times 15\,000 = 780\,000$ in this case (for each temperature). The value of the screening strength κ in Eq. (3) is chosen between 0 and 3 as suggested by previous experiments [15,16,41,42]. The results presented here are for $\kappa = 2$. The particularly chosen value of κ barely influences the results (see below for error ranges).

The corresponding density of states ρ according to Eq. (4) is obtained and shown in Fig. 2 for four temperature values [here, by convention, the unstable branch $\rho_u(|\omega|)$ is shown on the negative frequency axis]. The lowest temperature shown in this figure is already decisively larger than room temperature, but ρ shows a very peaked structure indicating that only certain modes at specific frequencies can occur in this ordered state. For example, the peak at $\omega/\omega_0 \approx 2$ corresponds to the breathinglike mode at $\kappa = 2$, where all particles oscillate (nearly) radially inward and outward (for pure Coulomb interaction the breathing mode [43] is found at $\omega = \sqrt{3}\omega_0$ [32], but the frequency increases with increased screening [16,35]).

This state density very much resembles that found for the solid ground state [32,44], except for the small unstable part. Corresponding particle trajectories at different temperature are indicated in Fig. 3. For higher temperatures, a more continuous mode spectrum $\rho(\omega)$ is found, reflecting the disordered arrangement. Nevertheless, breathing-mode-like oscillations

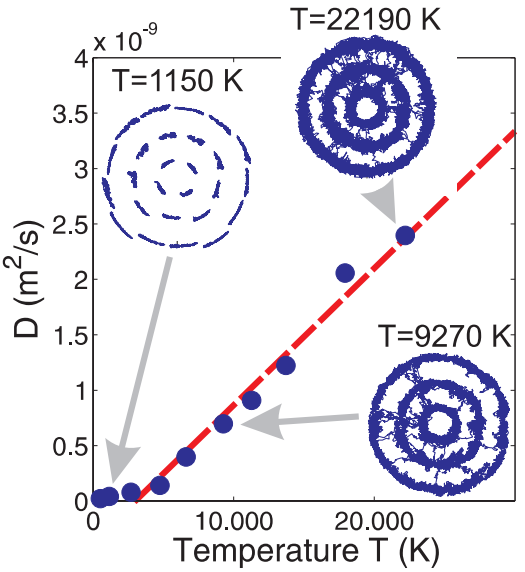

FIG. 3. (Color online) Diffusion coefficient D derived from INM analysis as a function of cluster temperature. A linear fit to the data $D(T)$ is also indicated. The insets show the trajectories of the particles in the cluster with $N = 26$ at different temperatures.

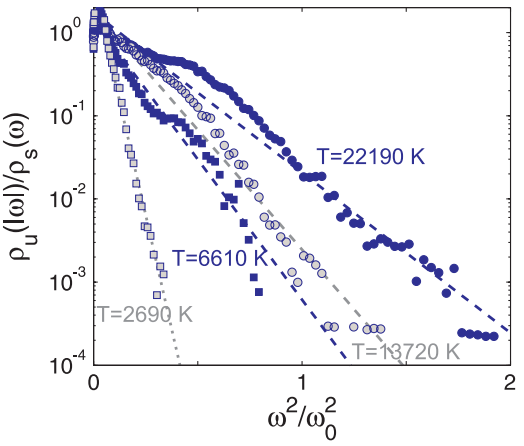

FIG. 4. (Color online) The ratio $\rho_u(|\omega|)/\rho_s(\omega)$ as a function of ω^2 for $N = 26$ together with the best exponential fit at four different temperatures.

are still pronounced. As mentioned above, especially the unstable part of the state density ρ_u reflects the liquid behavior. The unstable part becomes much broader with increasing temperature. Also, the fraction of unstable modes compared to the total density increases from about 2% to about 6%. These findings already qualitatively demonstrate the change from a solidlike to a liquidlike cluster (see below or Ref. [40]). In this section, *all* modes with imaginary ω_ℓ are counted and no distinction into double-well or escape modes is made. The behavior of DW and escape modes is discussed in Sec. IV D in more detail.

The diffusion constant derived from the INM technique is shown in Fig. 3. The diffusion constant is calculated from Eq. (5) using the hopping rate from Eq. (7). For that purpose, the ratio of the unstable and stable branch of the density of states $\rho_u(|\omega|)/\rho(\omega)$ is fitted to the exponential function $A\exp(-B\omega^2/kT)$ [30]. The quality of the fit can be judged from Fig. 4, in which the ratio together with the best fits are shown for different temperatures. It is seen that the overall agreement with the exponential form is reasonable. The exponential decay is strongest for the lower temperatures. Correspondingly, this reflects the broader unstable part already seen in the density of states in Fig. 2 at higher temperatures. It should be noted that for the lowermost temperatures near room temperature, fitting to an exponential decay was not always possible. This might be taken as a hint that at these temperatures the cluster is in a solid state.

The so-derived diffusion constants in Fig. 3 increase nearly linearly when a threshold temperature is exceeded. Such a behavior has also been reported from diffusion processes in simulations of extended 3D Yukawa systems [45,46]. The diffusion constant in our experiments takes values up to $D = 3 \times 10^{-9}$ m^2/s. For extended 2D systems under similar conditions, values in the range $D = 10^{-9}$–10^{-7} m^2/s [47–49] were reported.

The diffusion constants acquired by INM are now extrapolated to $D \to 0$ to identify the "freezing point", thereby assuming that in the solid regime the diffusion constant is much smaller than in the liquid. The so-achieved "freezing" temperature is the so-called mode-coupling temperature T_c that, in extended systems, is associated with the solid-liquid transition temperature T_m, where $T_c \leqslant T_m$ [50]. Here, we define the measured T_c as the freezing transition temperature that is approached from the liquid phase of the cluster. For the discussed cluster with $N = 26$, we derive from Fig. 3 a freezing temperature of $T_c = 2900$ K.

To assess the errors connected with the INM analysis, we have calculated the diffusion constants using different values of the screening strength κ in Eq. (3) in the evaluation of the energy. Figure 5 shows the diffusion constants for values of $\kappa = 0$ to 3. It can be seen that the diffusion constants depend only slightly on κ. Similarly, the freezing temperatures T_c change by only 10% for the different screening strengths.

In conclusion, the INM diffusion analysis now allows us to assign a freezing temperature, indicating a fluid-to-solid phase

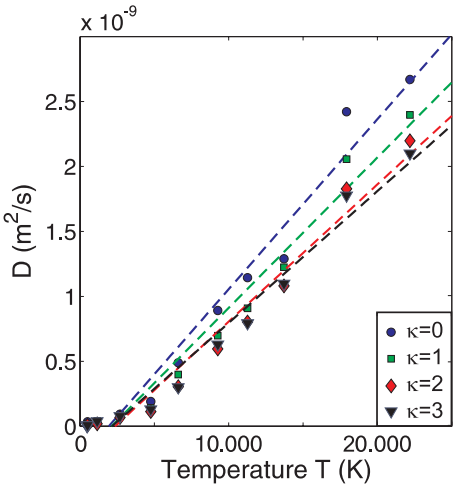

FIG. 5. (Color online) Diffusion constants derived from INM as a function of temperature for different values of the screening strength κ in Eq. (3).

transition, at the point where the liquid properties are lost. In complementary approaches, e.g., the interparticle distance fluctuations [25], one usually is interested in identifying the loss of order to search for the solid-to-fluid transition. As mentioned above, in the INM approach at each time step all $2N$ eigenfrequencies ω_ℓ enter the analysis, yielding a quite high statistical quality.

B. Comparison to other techniques

It is now certainly of enormous interest to compare the diffusion constants derived by INM to those using other techniques. The standard way to derive diffusion constants is via the mean-squared displacement (MSD) $\langle|\vec{r}_i(t) - \vec{r}_i(0)|^2\rangle$ [51–54] as

$$D = \lim_{t\to\infty} \frac{1}{4t}\langle|\vec{r}_i(t) - \vec{r}_i(0)|^2\rangle. \tag{8}$$

Under normal diffusion, the MSD scales linearly with time t for times $t \gg \omega_0^{-1}$; for short times t ballistic transport is expected where MSD scales as t^2. The diffusion constant D then is the slope of the MSD in the linear regime. Clearly, this reasoning holds in particular for extended systems. Alternatively (see, e.g., Refs. [53,55]), the diffusion coefficient can be derived from the velocity autocorrelation function (VACF) $Z(t) = N^{-1}\langle|\vec{v}_i(t)\cdot\vec{v}_i(0)|^2\rangle$ via

$$D = \frac{1}{2}\int_0^\infty Z(t)\,dt. \tag{9}$$

Both Eqs. (8) and (9) are given here for two-dimensional systems.

Figure 6(a) shows the behavior of the mean-squared displacement over time for our finite dust cluster with $N = 26$ at a temperature well in the liquid regime at $T = 9270$ K. For times up to $t \approx 0.1$ s we find a ballistic regime. For larger times, no clear dependence can be observed. The scaling MSD $\propto t^\alpha$ is somewhere between linear ($\alpha = 1$) and less than linear ($\alpha < 1$). This makes it difficult to assign a clear linear regime and thus to determine a diffusion constant. Clearly, the finite system size of the order of a few mm limits the diffusive behavior of the particles to values of the MSD $\approx 10^{-5}$ m^2, resulting in the weak scaling and oscillatory behavior of the MSD for large times t.

A further aspect that needs to be taken into account for our experimental system is the fact the particle motion is hindered by friction with the neutral gas in the discharge. Certainly, friction also affects the particles' diffusive behavior.

Vaulina *et al.* [55] have quantitatively addressed the diffusion behavior of particles in a trap under the influence of friction in terms of the time-dependent diffusion constant $D(t) = \langle|\vec{r}_i(t) - \vec{r}_i(0)|^2\rangle/(4t)$. Figure 6(b) shows the measured time-dependent diffusion constant $D(t)$ in comparison to the model [55] for the experimental parameters of friction coefficient $\beta \approx 5$ s^{-1} and trap frequency $\omega_0/(2\pi) \approx 0.8$ s^{-1}. In the model, D_0 is the diffusion constant of a freely diffusing system. The two curves are in quite nice agreement, indicating the validity of the approach.

To compare now with the diffusion from INM, we derived on the one hand the diffusion constant from the VACF, and

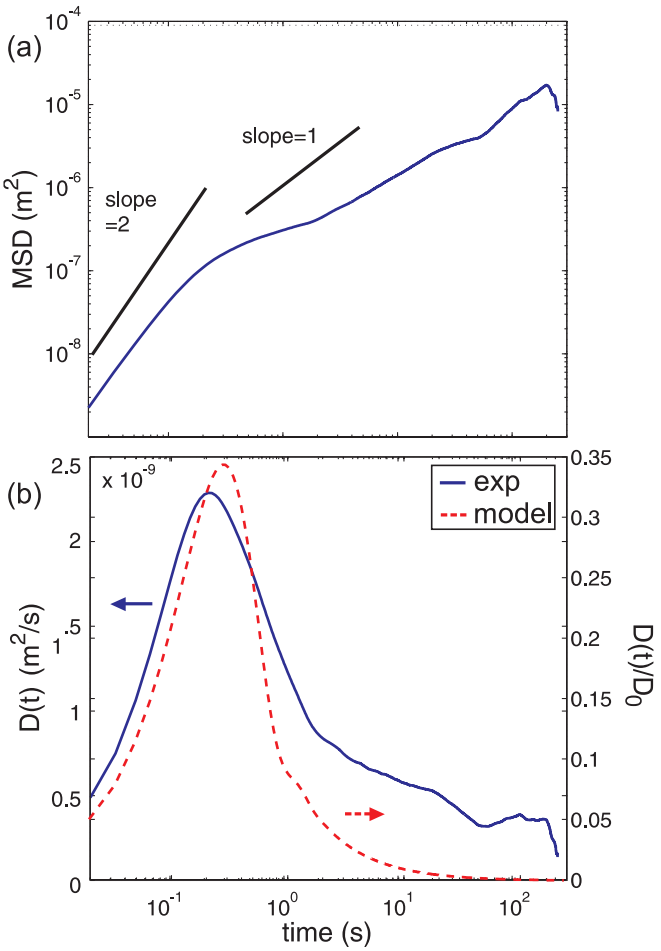

FIG. 6. (Color online) (a) Mean-squared displacement MSD over time for $N = 26$ at a temperature of $T = 9270$ K. (b) Corresponding time-dependent diffusion constant $D(t)$ derived from the experiment (solid line). A model calculation according to Ref. [55] is shown for comparison.

on the other hand from the maximum of the time-dependent MSD diffusion constant. The so-derived diffusion constants are compared to those from INM in Fig. 7. There is a gross agreement between the diffusion constants from INM, MSD, and VACF. Both the VACF and time-dependent MSD diffusion values exceed those from INM. Since the MSD values are the *maximum* of the time-dependent diffusion constant, it is not surprising that they are generally larger than the INM values. Further, the VACF values show a much stronger scatter than the INM values, especially at low temperatures, and seem to be shifted upward on the ordinate compared to the INM and MSD values. One reason for that behavior might be that the particle velocities entering the calculation of the VACF are derived from the difference in particle position of successive frames, and any small errors in position result in larger errors for the velocities. Neither VACF nor time-dependent MSD indicate a threshold behavior with temperature. Instead, a more or less continuous increase of the diffusion constant with temperature is seen. Hence, a melting temperature cannot be derived from VACF and MSD diffusion coefficients.

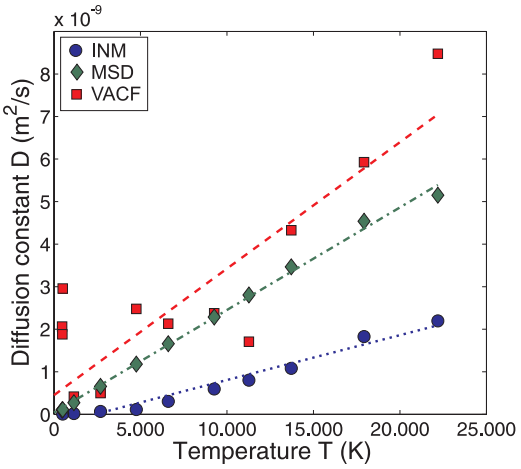

FIG. 7. (Color online) Diffusion constants derived from MSD, VACF, and INM (symbols) as a function of temperature, respectively. The lines indicate best linear fits to the diffusion constants where the dashed, dash-dotted, and dotted lines are the fit to VACF, MSD, and INM values, respectively.

C. Comparison to simulations

We have performed Langevin molecular-dynamics simulations of 2D dust clusters at different temperatures. The Langevin technique accounts for velocity-dependent damping and random kicks to mimic the neutral-gas friction of the particles and the heating by random laser forces. The particles were modeled according to Eq. (3) to be trapped in a harmonic 2D confinement interaction with a screened Coulomb potential with $\kappa = 2$. Then a time series for particle motion in the simulation corresponding to 15 000 "frames" has been determined for various temperatures of the cluster. Then, as in the experiment, the INM analysis has been performed and the freezing temperatures (i.e., the mode-coupling temperatures T_c) have been derived from the extrapolation of the diffusion constants $D \to 0$, as described above.

In the experiment, the corresponding freezing temperatures have been derived for a number of different dust cluster with particle numbers between $N = 19$ and 50. These freezing temperatures are shown in Fig. 8 as a function of particle number N. The error bars take into account the uncertainty due to the chosen values of κ and c in Eqs. (3) and (7). Similarly, simulations have been performed for the same clusters as in the experiment, and the derived freezing temperatures are also given in Fig. 8.

One finds a close agreement of the temperatures with the simulated and the experimental clusters, especially for the smaller clusters. The discrepancies for larger clusters are due to the fact that the exact cluster configurations in experiment and simulation generally are different. This is because with a larger particle number many more metastable configurations exist that have only slightly larger energy than the ground state. We found that some of the experimental configurations indeed correspond to metastable configurations. Since the mode-coupling (freezing) temperature is sensitive to the cluster configuration, the observed differences in melting temperature may well arise.

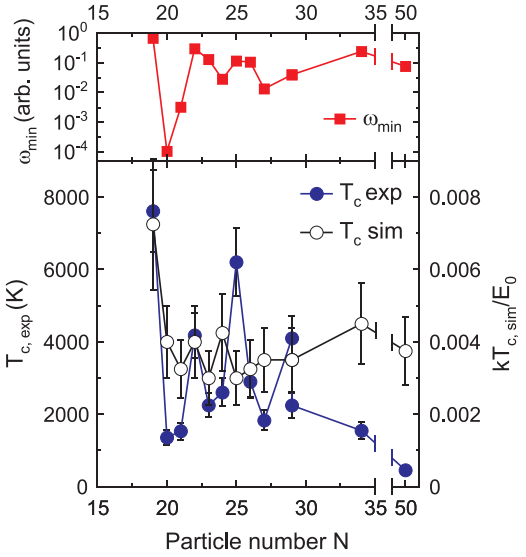

FIG. 8. (Color online) Freezing temperature of dust clusters with different particle number N. Shown are temperatures from the experiment and from simulated dust clusters. The upper panel shows the frequency of the least stable mode from Ref. [32].

For comparison, we also have plotted the frequency of the least stable mode as determined from the ground-state configuration by Schweigert *et al.* [32]. The least stable mode, i.e., the mode of lowest eigenfrequency ω_ℓ, reflects the symmetry and the configurational stability of these 2D clusters [32,56]. A paradigm in this context are the clusters with $N = 19$ and 20. The 19-cluster has a configuration (1,6,12) where 1 particle is in the center, 6 particles are in the inner ring, and 12 particles in the outer ring. This configuration is of high symmetry due to the commensurate number of particles in the inner and outer rings. Moreover, it has the hexagonal arrangement expected for infinite 2D systems. The 20-cluster is of (1,7,12) configuration with correspondingly low symmetry. Consequently, from the experimental INM analysis the freezing temperature is derived for $N = 19$ as very high ($T_c = 7600$ K), whereas for $N = 20$ it is found very low ($T_c = 1360$ K). For almost all investigated clusters, the least stable mode frequency is very well correlated with the freezing temperature [26].

D. Double-well and escape modes

We have seen in Fig. 2 that the fraction of unstable modes grows with temperature. This is quantified in Fig. 9(a) where the fraction of unstable modes $f_u = \int_0^\infty \rho_u(|\omega|)d\omega$ in relation to the fraction of stable modes $f_s = \int_0^\infty \rho_s(\omega)d\omega$ is shown as a function of temperature. In Fig. 9(a), all modes with imaginary mode frequency have been used to measure f_u. At low temperatures, this fraction f_u/f_s is about 2% and increases to about 6.5% at $T = 20\,000$ K.

To further characterize the unstable branch ρ_u, we have calculated the double-well and the escape INM modes as described above. The respective fractions f_u/f_s as a function of temperature are shown in Figs. 9(b) and 9(c), where only DW modes and escape modes, respectively, are used to determine f_u. It is seen that the fraction of DW modes is smaller by about

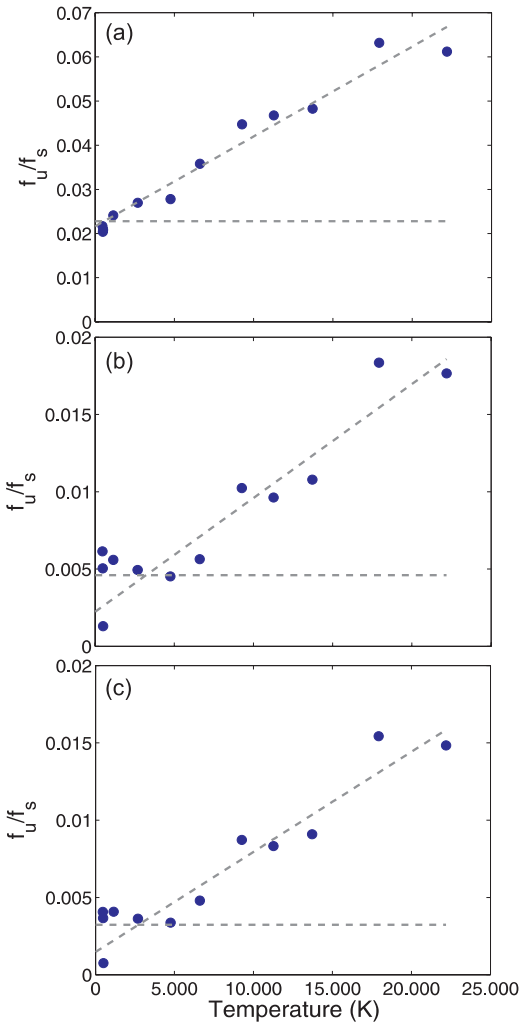

FIG. 9. (Color online) Ratio of the density of states f_u/f_s for a cluster with $N = 26$ at different temperatures. In (a) all INM modes are used, in (b) only DW modes, and in (c) only escape modes.

a factor of 4 compared to Fig. 9(a), indicating that only every fourth unstable mode is a DW mode. The others are single-well modes with a shoulder of negative curvature. The escape mode fraction, in turn, is only slightly smaller than the DW mode fraction. This indicates that the two wells of the DW modes indeed belong to different configurations. Such a behavior has been previously revealed for simulations of extended liquids (water) [57].

It has also been shown that the DW and escape mode fraction closely follows the behavior of the diffusion constant [57]. Indeed, the mode fraction shows a kink at a certain temperature: while for smaller temperatures f_u/f_s is nearly constant, a linear increase is seen for higher temperatures. We have therefore applied a linear fit to the mode fraction ratio for higher temperatures and tried to identify the point where it bends over to the constant part (see dashed lines in Fig. 9). It is seen that the transition temperature T_t is about 3000 K and thus very close to the freezing, i.e., mode-coupling, temperature T_c derived from the extrapolation of the diffusion constant. The comparison of derived temperatures is shown quantitatively in Table I.

TABLE I. Comparison of freezing temperature T_c derived from the extrapolation of the diffusion constant and the temperature T_t at which the mode ratio f_u/f_s bends over to a constant value. The errors for the temperatures are about 20%.

Considered modes	T_c (K)	T_t (K)
all INM modes	2900	600
DW modes only	2970	3230
escape modes only	2940	2730

Clearly, the freezing temperatures T_c and transition temperatures T_t agree within about 10% when DW modes or escape modes are considered. Taking all unstable INM modes, a reliable temperature T_c is still derived from the extrapolation of the diffusion constant, but the f_u/f_s ratio is not a good indicator. This is again in agreement with findings for simulated extended liquids [57]. Our investigations extend this finding and show the usefulness of this approach also for finite systems under experimental conditions.

E. Characterization of modes

Finally, we will characterize the nature of the modes to elucidate whether the above measured freezing temperatures are connected to radial or angular loss of order. Because normal modes in finite systems cannot be separated into purely compressional or shear motion, the respective compressional and shear contribution to each mode is calculated. This is done via the local divergence for the compressional contribution ψ_c and the local rotor for the shear contribution ψ_s according to [32,56]

$$\psi_c = \frac{1}{N}\sum_{i=1}^{N}\psi_{c,i}^2, \qquad \psi_s = \frac{1}{N}\sum_{i=1}^{N}\psi_{s,i}^2, \tag{10}$$

with

$$\psi_{c,i} = \sum_{j=1}^{M}(\vec{r}_i - \vec{r}_j)\cdot(\vec{e}_{i,\ell} - \vec{e}_{j,\ell})/|\vec{r}_i - \vec{r}_j|^2, \qquad \psi_{s,i} = \sum_{j=1}^{M}|(\vec{r}_i - \vec{r}_j)\times(\vec{e}_{i,\ell} - \vec{e}_{j,\ell})|/|\vec{r}_i - \vec{r}_j|^2, \tag{11}$$

where $\vec{r}_j$ are the positions of the neighbors of particle i, and M is the number of neighbors.

The compressional and shear contributions of all INM modes have been determined accordingly. The relative abundance of modes at frequency ω with the compressional contribution ψ_c or the shear contribution ψ_s is given in Fig. 10 for the highest temperature ($T = 22\,190$ K) realized in the $N = 26$ cluster. First, it is seen that for each mode frequency, the compressional and shear contributions are concentrated in a narrow band. This shows that each frequency contains very similar mode patterns. Second, the shear contribution is large for low-frequency modes with $|\omega/\omega_0| < 2$ whereas the high-frequency modes ($\omega/\omega_0 > 3$) are dominated by more

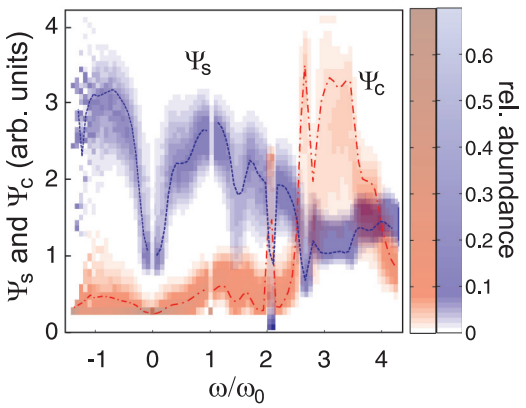

FIG. 10. (Color online) Plane of mode frequency ω and compressional part ψ_c and shear part ψ_s, respectively, for the $N = 26$ cluster at $T = 22\,190$ K. Darker colors indicate a higher abundance of modes. To guide the eye, the lines indicate the mean values of ψ_c (dash-dotted) and ψ_s (dashed).

compressional modes. Similar findings have been made for equilibrium normal mode analysis of dust clusters [16]. Such a behavior is expected since compressional modes lead to changes in interparticle distances and thus to stronger restoring forces and thus to higher-frequency oscillations.

Interestingly, the unstable branch (on the negative frequency axis) supports practically only pure shear modes with essentially no compressional contribution. Hence, especially those shearlike modes are connected with the liquid behavior of the cluster. This is plausible since the melting of finite clusters happens in two steps, whereby angular melting precedes the radial melting [20,21,32,56,58]. Naturally, angular motion is preferably shearlike and radial motion preferably compressional. Hence, the dominance of the shear contribution in the unstable branch suggests the priority of angular melting here.

V. CONCLUSION AND SUMMARY

We have analyzed the solid-to-liquid transition in finite two-dimensional dust clusters using the method of instantaneous normal modes. This technique was originally developed to address the fluid state of (simulated) liquids [28,29]. Here, we have applied it to long-term observations of experimental finite dust systems that were laser-heated from a solid to a liquid state.

First, from the INMs we retrieved liquid state properties such as the diffusion constant, which was found to increase nearly linearly above a temperature threshold. This temperature threshold T_c can then be taken as a freezing temperature of the cluster. This has been substantiated by Langevin simulations of dust ensembles with the same particle number.

We then analyzed the unstable modes and the role of topological mode filtering (all unstable modes, double-well modes, and escape modes). We found that the behavior of the DW modes and the escape modes reflects very well the behavior of the diffusion constant and the freezing temperatures. Hence, the mode-coupling temperature T_c derived from the zero-crossing of the diffusion constant and the transition temperature T_t from the bending-over of the f_u/f_s ratio both qualify as a "freezing" temperature. Further, the shear and compressional contributions of the stable and unstable modes were analyzed, revealing that the unstable modes are preferably shearlike modes, which corresponds very well to the orientational melting of finite clusters.

Finally, the diffusion constants derived from INM have been checked against those that are usually determined from an evaluation of the mean-squared displacement or the velocity autocorrelation function. Here, however, the mean-squared displacement is not a good indicator of the diffusion constant since the diffusive regime is not really entered because of the finite system size. The diffusive motion is hindered by the confinement. The same applies to the analysis using the velocity autocorrelation function.

In contrast, the INM technique looks at the momentary configuration and its small-scale motion to derive the properties of the system and hence allows us to extract valuable information even from a finite system. Moreover, the INM technique, in contrast to other measures such as the Lindemann criterion, focuses on the liquid side of the phase transition, and the phase change is attributed to the point where the liquid properties are lost.

In summary, the INM provides additional insight into the phase behavior of finite dust systems.

ACKNOWLEDGMENTS

We thank M. Bonitz and P. Ludwig (ITAP, University Kiel) for fruitful discussions and gratefully acknowledge financial support from DFG under Grant No. SFB-TR24, project A2 and A3.

[1] J. H. Chu and L. I, Phys. Rev. Lett. **72**, 4009 (1994).
[2] H. Thomas, G. E. Morfill, V. Demmel, J. Goree, B. Feuerbacher, and D. Möhlmann, Phys. Rev. Lett. **73**, 652 (1994).
[3] Y. Hayashi and K. Tachibana, Jpn. J. Appl. Phys. **33**, L804 (1994).
[4] A. Homann, A. Melzer, S. Peters, and A. Piel, Phys. Rev. E **56**, 7138 (1997).
[5] A. Homann, A. Melzer, R. Madani, and A. Piel, Phys. Lett. A **242**, 173 (1998).
[6] K. Takahashi, T. Oishi, K. I. Shimomai, Y. Hayashi, and S. Nishino, Phys. Rev. E **58**, 7805 (1998).
[7] A. Melzer, Plasma Sources Sci. Technol. **10**, 303 (2001).
[8] B. Liu, J. Goree, V. Nosenko, and L. Boufendi, Phys. Plasmas **10**, 9 (2003).
[9] M. Wolter and A. Melzer, Phys. Rev. E **71**, 036414 (2005).
[10] V. Nosenko, J. Goree, and A. Piel, Phys. Plasmas **13**, 032106 (2006).
[11] J. Schablinski, D. Block, A. Piel, A. Melzer, H. Thomsen, H. Kählert, and M. Bonitz, Phys. Plasmas **19**, 013705 (2012).
[12] H. Thomsen, H. Kählert, M. Bonitz, J. Schablinski, D. Block, A. Piel, and A. Melzer, Phys. Plasmas **19**, 023701 (2012).

[13] W.-T. Juan, Z.-H. Huang, J.-W. Hsu, Y.-J. Lai, and L. I, Phys. Rev. E **58**, 6947 (1998).
[14] M. Klindworth, A. Melzer, A. Piel, and V. A. Schweigert, Phys. Rev. B **61**, 8404 (2000).
[15] A. Melzer, M. Klindworth, and A. Piel, Phys. Rev. Lett. **87**, 115002 (2001).
[16] A. Melzer, Phys. Rev. E **67**, 016411 (2003).
[17] F. M. H. Cheung, C. Brunner, A. A. Samarian, and B. W. James, in *AIP Conference Proceedings No. 799* ("New vistas in dusty plasmas"), edited by L. Boufendi, M. Mikikian, and P. K. Shukla (AIP, New York, 2005), p. 185.
[18] O. Arp, D. Block, A. Piel, and A. Melzer, Phys. Rev. Lett. **93**, 165004 (2004).
[19] T. Antonova, B. M. Annaratone, D. D. Goldbeck, V. Yaroshenko, H. M. Thomas, and G. E. Morfill, Phys. Rev. Lett. **96**, 115001 (2006).
[20] A. Schella, T. Miksch, A. Melzer, J. Schablinski, D. Block, A. Piel, H. Thomsen, P. Ludwig, and M. Bonitz, Phys. Rev. E **84**, 056402 (2011).
[21] V. M. Bedanov and F. M. Peeters, Phys. Rev. B **49**, 2667 (1994).
[22] S. Apolinario, B. Partoens, and F. Peters, New J. Phys. **9**, 283 (2007).
[23] S. W. S. Apolinario, B. Partoens, and F. M. Peters, Phys. Rev. B **77**, 035321 (2008).
[24] J. P. Schiffer, Phys. Rev. Lett. **88**, 205003 (2002).
[25] J. Böning, A. Filinov, P. Ludwig, H. Baumgartner, M. Bonitz, and Y. E. Lozovik, Phys. Rev. Lett. **100**, 113401 (2008).
[26] A. Melzer, A. Schella, J. Schablinski, D. Block, and A. Piel, Phys. Rev. Lett. **108**, 225001 (2012).
[27] G. Seeley and T. Keyes, J. Chem. Phys. **91**, 5581 (1989).
[28] R. M. Stratt, Acc. Chem. Res. **28**, 201 (1995).
[29] T. Keyes, J. Phys. Chem. A **101**, 2921 (1997).
[30] G. V. Vijayadamodar and A. Nitzan, J. Chem. Phys. **103**, 2169 (1995).
[31] J. D. Gezelter, E. Rabani, and B. J. Berne, J. Chem. Phys. **107**, 4618 (1997).
[32] V. A. Schweigert and F. M. Peeters, Phys. Rev. B **51**, 7700 (1995).
[33] Y. Cornelissens, B. Partoens, and F. M. Peeters, Physica E **8**, 314 (2000).
[34] T. E. Sheridan, Phys. Rev. E **72**, 026405 (2005).
[35] C. Henning, K. Fujioka, P. Ludwig, A. Piel, A. Melzer, and M. Bonitz, Phys. Rev. Lett. **101**, 045002 (2008).
[36] Y.-J. Lai and L. I, Phys. Rev. E **60**, 4743 (1999).
[37] H. Totsuji, Phys. Plasmas **8**, 1856 (2001).
[38] T. Keyes, G. V. Vijayadamodar, and U. Zurcher, J. Chem. Phys. **106**, 4651 (1997).
[39] Z. Donkó, G. J. Kalman, and K. I. Golden, Phys. Rev. Lett. **88**, 225001 (2002).
[40] R. Schulz, M. Krishnan, I. Daidone, and J. C. Smith, Biophys. J. **96**, 476 (2009).
[41] S. Käding, D. Block, A. Melzer, A. Piel, H. Kählert, P. Ludwig, and M. Bonitz, Phys. Plasmas **15**, 073710 (2008).
[42] D. Block, S. Käding, A. Melzer, A. Piel, H. Baumgartner, and M. Bonitz, Phys. Plasmas **15**, 040701 (2008).
[43] A strict breathing mode with purely radial particle oscillations does not exist for Yukawa-type interactions. Nevertheless, almost identical breathinglike oscillation patterns are found [25]. These breathinglike modes are meant, here.
[44] K. Nelissen, A. Matulis, B. Partoens, M. Kong, and F. M. Peeters, Phys. Rev. E **73**, 016607 (2006).
[45] H. Ohta and S. Hamaguchi, Phys. Plasmas **7**, 4506 (2000).
[46] S. A. Khrapak, O. S. Vaulina, and G. E. Morfill, Phys. Plasmas **19**, 034503 (2012).
[47] O. Vaulina and S. V. Vladimirov, Phys. Plasmas **9**, 835 (2002).
[48] B. Liu and J. Goree, Phys. Rev. Lett. **100**, 055003 (2008).
[49] L.-J. Hou, A. Piel, and P. K. Shukla, Phys. Rev. Lett. **102**, 085002 (2009).
[50] S. P. Das, Rev. Mod. Phys. **76**, 785 (2004).
[51] W.-T. Juan and L. I, Phys. Rev. Lett. **80**, 3073 (1998).
[52] B. Liu, J. Goree, and O. S. Vaulina, Phys. Rev. Lett. **96**, 015005 (2006).
[53] B. Liu and J. Goree, Phys. Rev. E **75**, 016405 (2007).
[54] T. Ott and M. Bonitz, Phys. Rev. Lett. **103**, 195001 (2009).
[55] O. S. Vaulina, X. G. Adamovich, O. F. Petrov, and V. E. Fortov, Phys. Rev. E **77**, 066403 (2008).
[56] M. Kong, B. Partoens, and F. M. Peeters, New J. Phys. **5**, 23 (2003).
[57] E. La Nave, A. Scala, F. W. Starr, F. Sciortino, and H. E. Stanley, Phys. Rev. Lett. **84**, 4605 (2000).
[58] Y. Ivanov and A. Melzer, Phys. Plasmas **12**, 072110 (2005).